Characterization of mesoporous carbons synthesized with SBA-16 silica template†

Tae-Wan Kim,[a] Ryong Ryoo,*[a] Kamil P. Gierszal,[b] Mietek Jaroniec,[b] Leonid A. Solovyov,[c] Yasuhiro Sakamoto[d] and Osamu Terasaki[d]

Received 11th November 2004, Accepted 4th February 2005
First published as an Advance Article on the web 14th February 2005
DOI: 10.1039/b417804a

The structure of ordered mesoporous carbons (OMC) synthesized with sucrose, furfuryl alcohol or acenaphthene using the SBA-16 mesoporous silica template with cubic $Im\bar{3}m$ structure has been investigated with X-ray powder diffraction (XRD), transmission electron microscopy (TEM), scanning electron microscopy (SEM) and N_2 adsorption. This work shows that, in contrast to carbons prepared from sucrose by using SBA-15 silica as template, the impregnation of SBA-16 with sucrose failed to produce OMC with cubic $Im\bar{3}m$ structure. However, when furfuryl alcohol and acenaphthene were used as carbon precursors, the cubic $Im\bar{3}m$ structure was retained in the products. Thus, the latter carbon precursors were more suitable than sucrose for the formation of rigidly interconnected carbon bridges through narrow apertures of the cage-like siliceous SBA-16 mesostructure. In particular, the use of furfuryl alcohol as carbon precursor allowed us to control the degree of mesopore filling in SBA-16 and consequently, to synthesize hollow or fully filled cage-like silica–carbon mesostructures as was done in the case of channel-like SBA-15. In the case of acenaphthene only fully filled mesostructures were formed but with a much higher degree of graphitization. In the present work, we took advantage of the recent developments in the synthesis of SBA-16 with tailored diameter and entrance size of mesopores and made a step forward in the fabrication of OMC by using cage-like mesoporous silicas with narrow interconnections as templates.

1. Introduction

In recent years, there was a growing interest in the synthesis of ordered mesoporous carbons (OMC) using porous inorganic templates.[1–8] Particularly, the synthesis of OMC that employs ordered mesoporous silicas (OMS) as templates has attracted much attention due to the structural ordering of pores, tailored porosity, high specific surface area, high stability and easiness of functionalization of the aforementioned mesostructures. These features shed light on future perspectives for the development of new adsorbents,[9,10] catalysts,[11] electrode materials[12–15] and templates for ordered mesoporous inorganic materials.[16,17] The OMS templates offered a big benefit from the viewpoint of structural order and diversity in achieving novel carbon structures. For example, MCM-48 mesoporous silica template with the cubic $Ia\bar{3}d$ structure[18,19] led to CMK-1 carbon with the $I4_1/a$ (or lower) structure[3,9,11–13,20,21] and CMK-4 with the $Ia\bar{3}d$ structure.[21,22] The SBA-1 silica template with the cubic $Pm3n$ structure[23,24] gave CMK-2 carbon (cubic $Pm3n$).[7,25] The SBA-15 template with the 2-dimensional (2-D) hexagonal $p6mm$ structure[26–30] was employed to synthesize CMK-3 ($p6mm$, rod-type framework)[16,17,31–38] and CMK-5 ($p6mm$, tube-type) carbons.[14,30,39–42] Recently, the large pore cubic $Ia\bar{3}d$ silica designated as KIT-6 gave CMK-8 (rod-type) and CMK-9 (tube-type) carbon with the same structural symmetry.[43–45]

Various carbon precursors such as sucrose, furfuryl alcohol, ethylene gas and *in-situ* polymerized phenol resin turned out to be suitable for the synthesis of ordered mesoporous carbons.[7,8,25] These organic substances after carbonization formed rigid carbon frameworks in the 3-D mesoporous network of the silica template. The structural order of the carbon frameworks was retained after silica template dissolution with NaOH or HF. It is noteworthy that two types of carbons with the same $p6mm$ mesostructural symmetry but different framework configurations, rod- and tube-types, respectively, were obtained when SBA-15 was used as template. The rod-type $p6mm$ mesoporous carbon, referred to as CMK-3, was synthesized by a complete filling of mesoporous cylindrical channels of the SBA-15 silica.[16,17,31–38] The other (CMK-5) carbon resulted from an incomplete filling of the SBA-15 channels, which after silica dissolution gave interconnected nanopipes.[14,30,39–42] These carbons exhibited a very short-range atomic order in the framework. More graphitic carbons were obtained *via* synthesis routes that utilize *in-situ* conversion of aromatic compounds into mesophase pitch inside silica templates or *via* direct use of the mesophase pitch as a carbon source.[46–48]

† Electronic supplementary information (ESI) available: Fig. 1S, 4S, and 5S showing N_2 adsorption–desorption isotherms for the SBA-16/carbon composites, the recovered SBA-16 samples obtained from the composites, and the carbon samples, respectively; Fig. 2S and 3S showing XRD patterns for the C_{FA1}-t carbons and the recovered SBA-16 samples obtained from the composites. See http://www.rsc.org/suppdata/jm/b4/b417804a/

*rryoo@kaist.ac.kr

As mentioned above, the SBA-15-templating synthesis of OMC can be controlled to produce either the tube- or rod-type carbon frameworks depending on the synthesis conditions. A similar result was achieved in the case of large-pore cubic $Ia\bar{3}d$ silica template (KIT-6) with a 3-D network of channel-like mesopores.[43] In addition to OMS with cylindrical mesopores, various mesoporous silicas with cage-like structures have been discovered in recent years, suggesting their potential application as templates for the synthesis of novel carbon mesostructures. In particular, recent development of the synthesis methods that employ the poly(ethylene oxide)-type block copolymers offered attractive opportunities for facile preparation of OMS with large cages.[24,26,49–51] The cage-like OMS may have the cubic $Im\bar{3}m$ structure (body-centered-cubic arrangement of cages with 8 apertures to the nearest neighbors as in SBA-16[24,26]) and the cubic $Fm3m$ structure (face-centered-cubic arrangement of cages, referred to as KIT-5[50]). These mesostructures have received much attention because of their 3-D connectivity (zeolite-like cages with dimensions in the mesopore region) and their potential applications for manufacturing gas sensors,[52] preparation of supported catalysts,[53–57] immobilization of biomolecules[58] and fabrication of nanostructured materials.[59]

Synthesis of OMC by using cage-like OMS as templates would lead to more interesting carbon nanostructures than those synthesized with the help of channel-like OMS because the former have narrow windows (or apertures) around cages. Particularly, from the viewpoint of the framework configuration, it would be interesting to learn whether the carbon replication with 'hollow' carbon nano-architectures is achievable in such cage-like OMS templates with narrow windows in addition to the fully filled mesostructures (similarly to CMK-5 *vs.* CMK-3 prepared with SBA-15). It was reported previously that the SBA-1[7,25] and SBA-16[60] mesoporous silicas were replicated to mesoporous carbons. However, the previous results were only briefly commented upon without detailed analysis of the framework structure. The lack of the structural analysis was due to the difficulty in the systematic synthesis of the carbon samples for large pore cage-like OMS having narrow pore apertures between adjacent cages (for example, apertures less than 2.3 nm in diameter for SBA-16 with 10 nm pores).[24] Since the small apertures make it difficult to form rigid carbon bridges between carbon nanoparticles prepared in silica cages, the synthesis of OMC by using cage-like OMS templates becomes progressively more difficult as the diameter of cage apertures decreases. Fortunately, the recently reported recipe allows one to synthesize the SBA-16 samples over a wide range of mesopore cage diameters and entrance sizes by employing block copolymer mixtures as templates and controlling synthesis temperature and time.[61] The possibility of tailoring the pore diameter and pore entrance size in SBA-16 opened new avenues for systematic studies of cage-like OMC with the $Im\bar{3}m$ structure.

In the present work, the SBA-16 synthesis route employing block copolymer mixtures as templates was exploited to prepare high-quality OMS templates for the synthesis of OMC. A series of the OMC samples was prepared under various synthesis conditions using sucrose, furfuryl alcohol and acenaphthene as carbon precursors. The resulting carbons were characterized by X-ray powder diffraction (XRD), transmission electron microscopy (TEM), scanning electron microscopy (SEM) and N_2 adsorption. This systematic study was undertaken to give an insight for the synthesis of highly ordered mesoporous carbons by using cage-like OMS templates that may be prepared in future in a wide variety of structures.

2. Experimental

2.1 Preparation of SBA-16 templates

Mesoporous silica materials with cubic $Im\bar{3}m$ structure were synthesized according to the procedure described elsewhere.[61] Briefly, two poly(alkylene oxide)-type triblock copolymers, P123 ($EO_{20}PO_{70}EO_{20}$, EO = ethylene oxide, PO = propylene oxide, MW = 5800, Aldrich) and F127 ($EO_{106}PO_{70}EO_{106}$, MW = 12600, Sigma) were dissolved together in aqueous HCl solution. Tetraethyl orthosilicate (TEOS, 98%, Acros) was added to the solution at 308 K, and magnetic stirring was continued for 15 min at the same temperature. The molar composition of the mixture was as follows: P123/F127/TEOS/HCl/H_2O = 1/2.3/621/2727/89182. This mixture was kept under static conditions in an oven for 24 h at the same temperature. Subsequently, the mixture was placed in an oven at 373 K for hydrothermal treatment, over a period ranging from 12 h to 7 d. After such hydrothermal aging, the solid product was recovered by filtration and dried at 373 K without washing. The resultant SBA-16 samples are denoted by SiO_2-*t* where *t* stands for the hydrothermal aging time (*t*) at 373 K. The samples were then washed with ethanol, dried in an oven at 373 K and calcined at 823 K. These siliceous samples were used as templates for carbon synthesis, directly or after Al incorporation. The Al incorporation was carried out with aqueous solution of $AlCl_3$ (Si/Al = 20) in the same way used for SBA-15.[53,62] The Al-incorporated samples are denoted by Al-SiO_2-*t*.

2.2 Synthesis of mesoporous carbons from various precursors

Sucrose. The OMC synthesis employing sucrose was the same as in our previous work on CMK-1,[3] except that the amounts of sucrose and sulfuric acid were changed in proportion to the mesopore volume. For example, SiO_2-1d possessed the total mesopore volume of 0.54 cm^3 g^{-1}. This sample was infiltrated with the carbon source twice. The first infiltration was performed with a mixture of 0.77 g sucrose, 0.047 mL H_2SO_4 and 2.5 g H_2O per g SiO_2. The second infiltration was with 0.495 g of sucrose, 0.03 mL of H_2SO_4 and 2.5 g of H_2O. The carbon/silica composite sample obtained after complete carbonization at 1173 K is denoted by C_{SU}/SiO_2-1d. The carbon product was recovered with HF solution as described previously. The mesoporous carbon is designated by C_{SU}-1d.

Furfuryl alcohol. Two different procedures were used to synthesize mesoporous carbons with 'hollow' and 'fully filled' mesopores, respectively, from furfuryl alcohol as carbon precursor. The procedure for hollow frameworks is essentially the same as that used for the synthesis of CMK-5 (2-D

hexagonal structure composed of carbon nanopipes) reported in previous works using Al-SBA-15 template,[14,30,39–42] except for the adjustment of the amount of carbon precursor in proportion to the pore volume (for example, 0.535 mL of furfuryl alcohol per g of Al-SiO_2-1d). This procedure may be briefly described as follows: initially furfuryl alcohol was infiltrated into calcined Al-SiO_2-*t* at room temperature and polymerized at 368 K. Heating of the resultant polymer/aluminosilicate composite at 1173 K under vacuum gave a carbon/aluminosilicate composite, from which the silica template was removed with HF. The carbon/aluminosilicate composites and corresponding carbons prepared according to this recipe are denoted by C_{FA1}/Al-SiO_2-*t* and C_{FA1}-*t*, respectively.

The second procedure was used to synthesize carbons by a complete filling of mesopores in SBA-16 by carbon precursor. In this procedure, infiltration and polymerization of furfuryl alcohol was repeated twice prior to carbonization. The latter was carried out under atmospheric pressure. The procedure for Al-SiO_2-1d can be briefly described as follows: the calcined aluminosilicate template was uniformly infiltrated with 0.535 mL furfuryl alcohol per g template at room temperature. The Al-SiO_2 sample containing furfuryl alcohol was placed in an oven at 308 K for 1 h and then at 373 K for 1 h. The resultant polymer/Al-SiO_2 composite sample was further heated for 2 h at 623 K. After the sample was cooled to room temperature, 0.268 mL furfuryl alcohol was added. This sample was heated at 373 and 623 K again. The final heating (carbonization) was done at 1173 K with the heating rate = 3.7 K min^{-1}. All heating treatments were performed under self-generated gas atmosphere using a quartz reactor equipped with a porous plug. The carbon/aluminosilicate composite and corresponding carbon obtained by this recipe are denoted by C_{FA2}/Al-SiO_2-1d and C_{FA2}-1d, respectively.

Acenaphthene. The carbon synthesis from acenaphthene is the same as that described in our previous work on CMK-3G,[46] except for the difference in the amount of carbon precursor (0.19 g of acenaphthene per 0.3 g of Al-SiO_2-1d). The synthesis recipe can be briefly described as follows: a physical mixture of acenaphthene and Al-SiO_2-1d was vacuum-sealed in quartz tubing and heated at 1023 K in a muffle furnace. After being cooled to room temperature, the product was moved into a fused quartz reactor, which was equipped with fritted disks. Carbonization was completed by heating the reactor at 1173 K under vacuum conditions. The carbon/aluminosilicate composite and corresponding carbon prepared by this recipe are denoted by C_{AC}/Al-SiO_2-1d and C_{AC}-1d, respectively.

2.3 Measurements

X-Ray diffraction (XRD) patterns were recorded on a Rigaku Multiplex instrument using Cu Kα radiation (λ = 0.15406 nm), operated at 50 kV and 30 mA (1.5 kW) in a step scan mode with narrow divergence slits. Synchrotron powder XRD data were collected using BL8C2 at Pohang Light Source in the reflection mode (λ = 0.14905 nm). Scanning electron micrographs (SEM) were obtained with a Philips SEM-535M microscope operating at the acceleration voltage of 20 kV. Silica samples were coated with gold before SEM measurements. Transmission electron microscopy (TEM) images were taken from thin edges of particles supported on a porous carbon grid, using JEOL JEM-3010 equipment operated at 300 kV. Nitrogen adsorption isotherms were measured at 77 K on a Micromeritics ASAP 2010 volumetric adsorption analyzer. Before the adsorption measurements, all samples were outgassed at 473 K in the port of the adsorption analyzer.

2.4 Calculations

The BET specific surface area[63] was calculated from nitrogen adsorption data in the relative pressure range specified in Tables 3 and 4 (later). The total pore volume[63] was estimated from the amount of nitrogen gas adsorbed at a relative pressure of about 0.98. The external surface area and the sum of the primary mesopore volume and the micropore volume were estimated from the nitrogen adsorption data using the α_s plot method[63,64] in the α_s range from about 1.7 to 2.5. The reference adsorption isotherm used in the α_s plot calculations was reported elsewhere.[64] The pore size distributions (PSD) were calculated from nitrogen adsorption isotherms using a method calibrated for MCM-41 silicas.[65,66] The position of the maximum on PSD is referred to as the pore diameter.

XRD structure analysis was performed by using the continuous density function (CDF)[67] technique with the structure model shown in Fig. 1. The density distribution in the materials was simulated by spherical areas of uniform density with the centers arranged in the vertices of the body centered cubic unit cell. No regular interconnections between the spherical areas were included into the simplified structural model since the available XRD data did not permit a comprehensive analysis of the interconnection system of the materials. The lattice parameters, sphere diameters, and sphere density were varied until the best fit for the diffraction pattern was obtained, by using a flexible model density function with

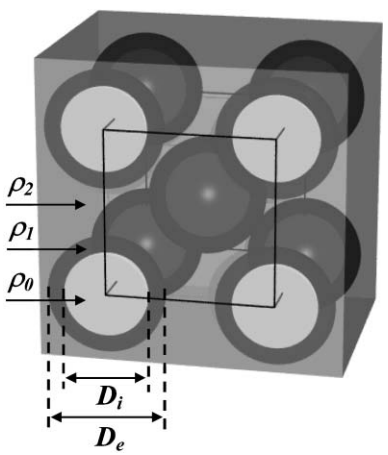

Fig. 1 Model of density distribution for SBA-16, filled carbon, and hollow carbon. The structure modeling was done with the following set of parameters: for SBA-16 D_e was varied, ρ_2 was fixed, ρ_0 was zero, D_i and ρ_1 were not used; for filled carbon D_e was varied, ρ_0 and ρ_2 were fixed, D_i and ρ_1 were not used; for hollow carbon D_e, D_i, and the ratio ρ_1/ρ_2 were varied, and ρ_0 was zero.

adjustable parameters. The intensities of the diffraction reflections were calculated from the numerical Fourier transform of the density function defined on a grid of the unit cell. The Debye–Waller factor was used to allow for the internal structural disorder. The adjustable parameters of the density function were refined by applying the derivative difference minimization[68] method, which allowed full-profile XRD refinement independently of the underlying background. The Rietveld[69] full-profile formalism was applied in the XRD powder profile simulations. The calculations were carried out using a computer code package based on a corrected and modified version of the Rietveld refinement program DBWS-9006PC.[70]

3. Results and discussion

3.1 SBA-16 silica template

The structure of SBA-16 consists of the body-centered-cubic arrangement of mesoporous spheres with 8 apertures to the nearest neighbors. The structure with 3-D pore connectivity looks perfect as a template that can retain the structural order in the resulting carbons. However, the outcome of this templating synthesis can be different since the diameter of the pore apertures depends significantly on the synthesis conditions and hydrothermal treatment. Therefore, we employed the synthesis conditions reported in our previous work on SBA-16 that assure largest possible pore apertures.[61] According to this synthesis procedure, a mixture of $EO_{20}PO_{70}EO_{20}$ and $EO_{106}PO_{70}EO_{106}$ block copolymers having an average formula $EO_{80}PO_{70}EO_{80}$ was used. In addition, the products were aged under the hydrothermal conditions at 373 K as described in section 2.1. It is noteworthy that the previous work reports several significant points regarding the synthesis of SBA-16 using $EO_{20}PO_{70}EO_{20}$ and $EO_{106}PO_{70}EO_{106}$ mixtures. Namely, the pore diameter and pore window size increased as the synthesis composition was changed from $EO_{106}PO_{70}EO_{106}$ to $EO_{80}PO_{70}EO_{80}$. Hydrothermal treatment or aging of the synthesis mixtures at 373 K led to the enlargement of pore diameters and pore windows.[61,71] In addition, the highest possible structural order for SBA-16, as judged by XRD, was obtained for $EO_{80}PO_{70}EO_{80}$ as the surfactant composition was varied from $EO_{20}PO_{70}EO_{20}$ to $EO_{106}PO_{70}EO_{106}$.

Fig. 2 shows the Cu Kα XRD pattern obtained for the Al-SiO_2-1d SBA-16 sample, which was calcined at 823 K after Al incorporation into the hydrothermally treated sample at 373 K for 1 d. The XRD pattern shows more than four well-resolved Bragg diffraction peaks at 2θ angles below 5°, which correspond to the cubic $Im\bar{3}m$ space group. Also, Fig. 2 shows SEM and TEM images for the SBA-16 silica sample. The SEM image indicates that the mostly observed particle morphology is that of rhombdodecahedron single crystal shape, which is in accordance with the crystal model of the cage-like $Im\bar{3}m$ structure.[72] The TEM image taken along [100] is shown in Fig. 2 together with corresponding Fourier diffractogram (FD), demonstrating the highly ordered cage-like arrangement of mesopores.

Shown in Fig. 3 is the XRD pattern obtained from the same SBA-16 sample (Al-SiO_2-1d, calcined and Al-incorporated)

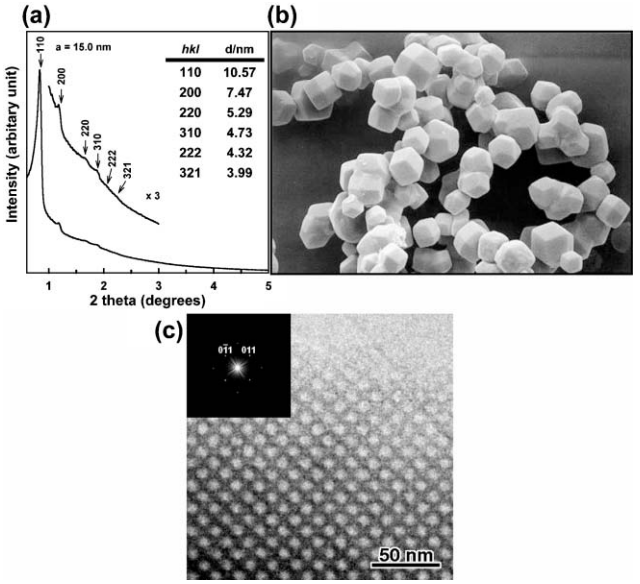

Fig. 2 (a) XRD pattern, (b) SEM image, and (c) TEM image for the SBA-16 mesoporous silica template synthesized with a mixture of triblock copolymers.

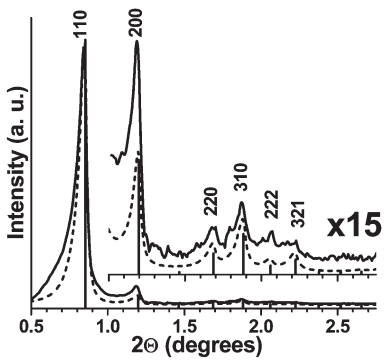

Fig. 3 Observed (solid line) and calculated (dotted line) synchrotron XRD profiles for the SBA-16 template. Calculated reflection positions are marked by vertical lines. The background curve is subtracted for clarity.

using synchrotron radiation and its best fit by the CDF modeling. Table 1 shows the structural parameters determined by the modeling of XRD data for the samples synthesized with various hydrothermal treatments and surfactant compositions. The XRD modeling data summarized in Table 1 are consistent with the previous study[61] of the effects of the surfactant composition and hydrothermal treatment on the resultant material structure. For example, the lattice parameter and the pore diameter increased with decreasing the EO block size and increasing the time of the hydrothermal treatment. The result also shows that the minimal distance between the surfaces of the neighboring cavities (w, used as a measure of the silica wall thickness) decreased gradually.

3.2 SBA-16/carbon composites

Fig. 4 shows Cu Kα XRD patterns for the composite samples. In the cases of C_{FA1}/Al-SiO_2-1d and C_{SU}/-SiO_2-1d the XRD

Table 1 Structural characteristics of SBA-16 templates determined by XRD modeling[a]

Sample	*a*/nm	D_e/nm	*w*/nm
SBA-16 using F127[b]	13.80	7.4	4.6
Al-SiO_2-12h[c]	14.79	8.6	4.2
Al-SiO_2-1d[c]	15.00	8.8	4.2
Al-SiO_2-3d[c]	15.65	9.6	4.0
Al-SiO_2-7d[c]	16.44	10.7	3.5

[a] a = the cubic lattice parameter; D_e = the external diameter of the spherical density area (Fig. 1); w = the minimal distance between the surfaces of the spherical density areas given by $(a\sqrt{3}/2-D_e)$. [b] SBA-16 silica synthesized using $EO_{106}PO_{70}EO_{106}$ alone. The molar composition of the synthesis mixture was: F127/TEOS/HCl/H2O = 3.0/757.1/3000/98100. Hydrothermal treatment was carried out at 373 K for 1 d. [c] SBA-16 silica synthesized using $EO_{80}PO_{70}EO_{80}$.

patterns are similar to those obtained for the corresponding silica templates. However, the (110) peak intensities for C_{FA2}/Al-SiO_2-1d and C_{AC}/Al-SiO_2-1d are much smaller in comparison to those observed for silica templates. The intensity losses for C_{FA2}/Al-SiO_2-1d and C_{AC}/Al-SiO_2-1d are similar to the cases of the carbon/silica composites of CMK-1 and CMK-3, which is due to the complete filling of pores in the silica template by carbon.[3,31] In particular, the almost total absence of the (110) peak for the C_{AC}/Al-SiO_2-1d sample indicates that the silica template pores not only were completely filled with carbon but also the carbon framework obtained from acenaphthene precursor is much denser than those obtained from sucrose and furfuryl alcohol. The XRD peak intensity for C_{SU}/SiO_2-1d was slightly decreased compared to that of the silica template, which indicates that the pores of SBA-16 may not be completely filled or are loosely packed with carbon when sucrose is used as carbon precursor. However, the peak intensity for C_{FA1}/Al-SiO_2-1d is enhanced in comparison to that observed for calcined SBA-16 silica template because the silica framework is coated with carbon film as in the CMK-5 silica/carbon composite.[40] Fig. 5 shows the synchrotron radiation XRD patterns and the corresponding simulated curves for the C_{FA1}/Al-SiO_2-*t* samples with various times of hydrothermal treatment. The XRD modeling results summarized in Table 2 for the C_{FA1}/Al-SiO_2-*t* samples show that the lattice parameter decreases slightly after carbonization in comparison to that for respective SBA-16 silica templates. However, the values of the lattice parameter, as well as diameters D_i and D_e, increase gradually with increasing time of the hydrothermal treatment, which is analogous to the case of the corresponding Al-SiO_2-*t* templates.

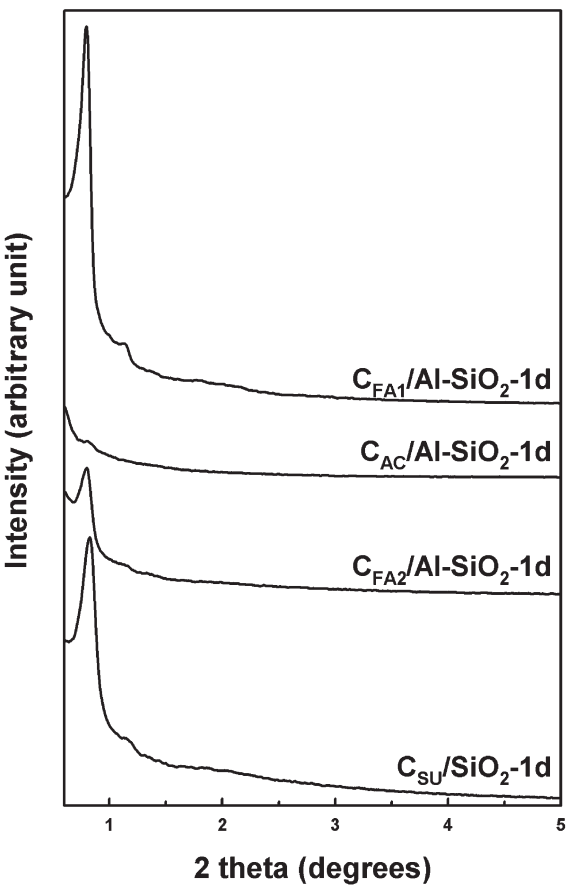

Fig. 4 XRD patterns for the SBA-16/carbon composites.

Nitrogen adsorption isotherms for the composites studied are shown in the ESI,† Fig. 1S. The composites with completely filled mesopores of SBA-16 by carbon precursor, C_{AC}/Al-SiO_2-1d and C_{FA2}/Al-SiO_2-1d, exhibit very low nitrogen uptake revealing inaccessibility of the internal pore space to the adsorbate. The adsorption isotherms for the samples, for which the silica surface is covered with carbon film, are considerably more pronounced. They feature hysteresis loops related to the capillary condensation–evaporation characteristic of mesoporous materials. The sizes of mesopores, which can be determined from the relative pressure that corresponds to the capillary condensation step as well as the volume of primary mesopores for the SBA-16 coated with furfuryl

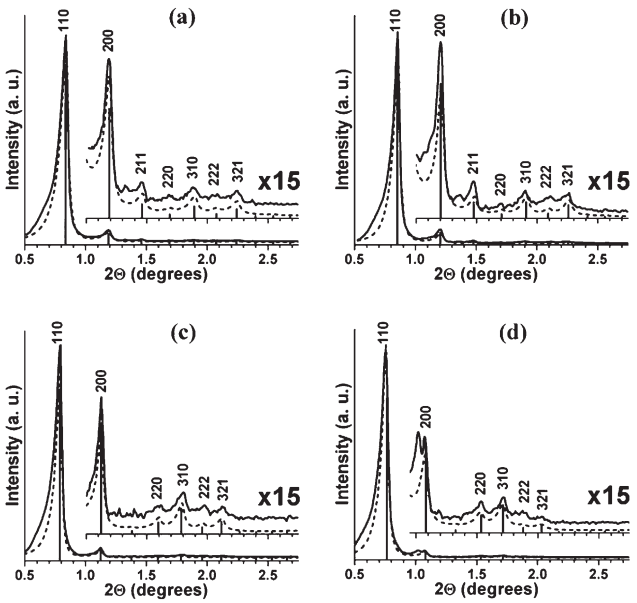

Fig. 5 Observed (solid line) and calculated (dotted line) synchrotron XRD profiles for the SBA-16/carbon composites: a) C_{FA1}/Al-SiO_2-12h, b) C_{FA1}/Al-SiO_2-1d, c) C_{FA1}/Al-SiO_2-3d, and d) C_{FA1}/Al-SiO_2-7d. Calculated reflection positions are marked by dotted lines. The background curve is subtracted for clarity.

Table 2 Structural characteristics of C_{FA1}/Al-SiO_2-*t* composites samples determined by XRD modeling[a]

Sample	*a*/nm	D_i/nm	D_e/nm	*w*/nm	*t*/nm	ρ_1/ρ_2
C_{FA1}/Al-SiO_2-12h	14.62	7.6	8.6[b]	4.1	0.51	0.7
C_{FA1}/Al-SiO_2-1d	14.61	7.7	8.8[b]	3.9	0.55	0.8
C_{FA1}/Al-SiO_2-3d	15.48	8.4	9.6[b]	3.8	0.61	0.7
C_{FA1}/Al-SiO_2-7d	16.19	8.8	10.7[b]	3.3	0.95	0.6

[a] *a* = the cubic lattice parameter; D_i and D_e = the internal and external diameters of the spherical density areas (Fig. 1), respectively; *w* = the minimal distance between the surfaces of the spherical density areas given by $(a\sqrt{3}/2 - D_e)$; *t* = the thickness of the carbon nanosphere walls given by $(D_e - D_i)/2$; ρ_2/ρ_1 = the ratio between the averaged scattering densities of the carbon nanosphere walls and the interconnecting carbon material between the nanospheres (Fig. 1). [b] The diameter D_e of the composite samples was constrained to be equal to that of the respective SBA-16 silica template (Table 1).

alcohol, increased for the composites from C_{FA1}/Al-SiO_2-12h to C_{FA1}/Al-SiO_2-7d with increasing time of the hydrothermal treatment.

The BET specific surface area and total pore volume for the composites with incompletely filled mesopores are in the range 280–420 $m^2\ g^{-1}$ and 0.17–0.24 $cm^3\ g^{-1}$ (Table 3), respectively, where the microporosity has a considerable contribution to both quantities. Their external surface areas estimated from α_s-plot analysis are remarkably small. These adsorption characteristics together with the TEM images for the SBA-16 silica templates show that the synthesized carbon/silica composites are of very good structural quality and exhibited negligible secondary porosity. On the basis of the hysteresis loop shape, specifically its evaporation branch, one can infer that the capillary evaporation occurred at the lower limit of adsorption–desorption hysteresis for nitrogen at 77 K, which, in this case, is at the relative pressure of about 0.4. This fact indicates the presence of constrictions in the porous network below 5 nm. Also, argon adsorption isotherms at 77 K were measured for those composites (data not shown) and showed the hysteresis closure at its lower limit (relative pressure about 0.3), which indicates the size of these constrictions is below 4 nm.[65]

Table 3 Structural properties for the SBA-16/carbon composites from nitrogen adsorption data[a]

Sample	S_{BET}/ $m^2\ g^{-1}$	S_{ex}/ $m^2\ g^{-1}$	V_t/ $cm^3\ g^{-1}$	$V_p + V_{mi}$/ $cm^3\ g^{-1}$	w_{KJS}/ nm
C_{SU}/SiO_2-1d	420	~0	0.22	0.22	5.70
C_{FA2}/Al-SiO_2-1d	5	5	0.01	—	—
C_{AC}/Al-SiO_2-1d	7	7	0.01	—	—
C_{FA1}/Al-SiO_2-12h	283	~0	0.17	0.16	5.35
C_{FA1}/Al-SiO_2-1d	364	~0	0.22	0.21	5.63
C_{FA1}/Al-SiO_2-3d	380	10	0.26	0.24	6.31
C_{FA1}/Al-SiO_2-7d	314	20	0.24	0.19	6.71

[a] S_{BET} = the BET specific surface area calculated in the range of relative pressures from 0.01 to 0.1; V_t = the total pore volume calculated at the relative pressure of about 0.98; $V_p + V_{mi}$ = the sum of the primary mesopore volume and micropore volume estimated by the α_s-plot method in the range of α_s from ~1.7 to 2.5; S_{ex} = the external surface area estimated by the α_s-plot method in the same range of α_s; w_{KJS} = the diameter of mesopores (formed by incomplete filling of the SBA-16 template) calculated using the KJS method.[64]

The pore size distributions (PSDs) for the SBA-16 composites (Fig. 6) show two main peaks that correspond to fine pores (below 3 nm) and primary mesopores of spherical shape (above 5 nm). The peak attributed to the fine pores is located at approximately constant value of the mean pore size for all composites with incompletely filled mesopores of SBA-16 and it reflects the intrinsic microporosity of furfuryl alcohol-based carbons. However, the peak related to the mesopores of SBA-16 coated with a furfuryl alcohol layer featured a gradual shift in the direction of larger pore diameters, *i.e.*, from about 5.3 to 6.7 nm. The pore size distribution analysis was performed using the KJS method calibrated for cylindrical mesopores.[66] Because the shape of the SBA-16 primary mesopores is spherical, one needs to keep in mind that the estimated pore size for the composites under study is underestimated by about 10–20%.

3.3 Mesoporous carbon materials

Shown in Fig. 7 are the XRD patterns for the carbon samples obtained by dissolving the silica template in the SBA-16/carbon composites. The XRD peak pattern for C_{FA1}-1d is

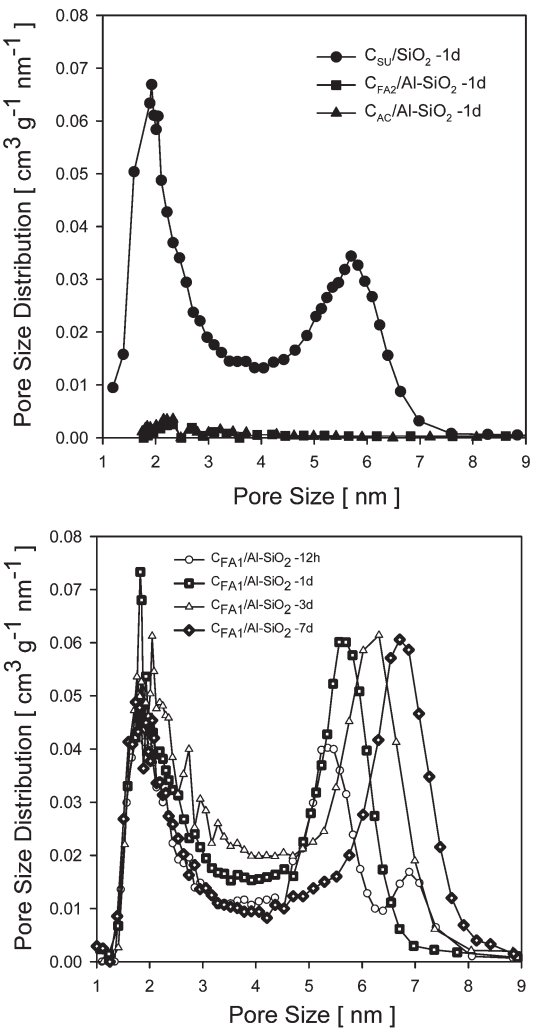

Fig. 6 Pore size distributions calculated from nitrogen adsorption isotherms for the SBA-16/carbon composites studied.

similar to that of its SBA-16 template. However, the XRD pattern for C_{SU}-1d is almost featureless after removal of the silica template with HF. The loss of structural ordering in the case of C_{SU}-1d indicates that sucrose is not an appropriate carbon precursor for the synthesis of cage-like cubic $Im\bar{3}m$ mesoporous carbons. Evidently, the carbon nanoparticles formed inside the SBA-16 pore cages were not fully interconnected with adjacent carbon particles due to the small size of connecting pores in the SBA-16 silica template and a sparse carbon framework formed during carbonization of sucrose. Therefore, it is difficult to form the 3-D network of interconnected carbon nanoparticles by infiltration and carbonization of sucrose in the SBA-16 template. In contrast, the XRD patterns for the C_{FA2}-1d sample are characteristic of the cubic $Im\bar{3}m$ space group even after removal of the silica template, which indicates that furfuryl alcohol is a suitable precursor for the synthesis of mesoporous carbons with the cage-like cubic $Im\bar{3}m$ structure and is able to infiltrate small pore connections in the SBA-16 template and to form a rigid 3-D carbonaceous mesostructure.

The C_{FA1}-1d carbon can also be indexed as a cage-like cubic $Im\bar{3}m$ structure, but in this case the silica removal led to significant changes in the XRD pattern. The main (110) peak intensity is reduced in comparison to two other peaks (200) and (211). The low (110) intensity for the cubic $Im\bar{3}m$ structure is similar to the loss of (10) peak intensity in the case of the 2-D hexagonal CMK-5.[14,30,39–42] These changes are attributed to empty carbon mesopores, which weaken the peak intensity by

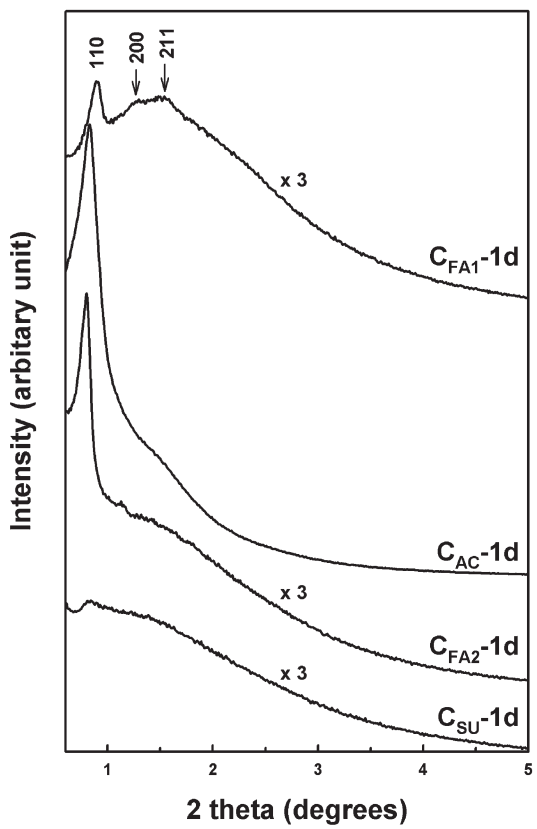

Fig. 7 Low angle XRD patterns for the carbon samples. The XRD patterns for C_{SU}-1d, C_{FA2}-1d and C_{FA1}-1d were multiplied by three.

interference of X-ray diffractions between inner and outer carbon walls. The C_{FA1}-1d carbon has two kinds of pores: the cage-like inner mesopores formed because of the incomplete filling of SBA-16 mesoporous cages and outer mesopores created after removal of the silica template walls. For this type of sample, the intensity of the (110) peak is reduced but the intensities of the (200) and (211) peaks increase with increasing time of the hydrothermal treatment (ESI† Fig. 2S).

In the case of C_{AC}-1d, the intensity of the (110) peak of the $Im\bar{3}m$ structure is high, but the other peaks are rather broad or disappear in comparison to the silica template. The high intensity of the (110) peak is caused by complete filling of the template pores with dense graphitic carbon through carbonization of *in-situ* generated mesophase pitch.[43] The broadening and disappearing of the other peaks suggests structural transformation of the silica template from a cage-like structure to a more open structure under the carbonization conditions at high temperature and auto-generated high pressure in the sealed quartz bulb. Fig. 3S and 4S in the ESI† show the XRD patterns and isotherms for the SBA-16 templates, which were obtained from the composites after burning off the carbon at 873 K for 5 h. The shapes of the XRD pattern and N_2 adsorption–desorption isotherm for the silica template recovered from the C_{AC}/Al-SiO_2-1d composite are markedly different from those for the original SBA-16 template.

Nitrogen adsorption isotherms for the carbons studied are shown in Fig. 5S (ESI†). In comparison to the composites, the synthesized carbons exhibit very high nitrogen adsorption. Thus, the template removal from the SBA-16/carbon composites creates additional pores in place of silica walls, which causes a noticeable increase in the total pore volume and BET specific surface area. The latter quantities are in the range 1.09–2.33 $cm^3\ g^{-1}$ and 1610–2050 $m^2\ g^{-1}$ for the carbons obtained from incompletely filled mesopores in SBA-16. These quantities are much lower for the carbons obtained by completely filled composites. For the former carbons, *e.g.*, C_{FA1}-7d, the nitrogen uptake is about 5 times higher and the total pore volume is almost 10 times greater than those for the corresponding composite (see Tables 3 and 4). Such a drastic difference indicates a quite substantial contribution arising from unfilled mesopores. The average ratio of the volume created after dissolution of silica walls to the internal volume of unfilled spherical mesopores is greater than that observed for the CMK-5 carbons reported earlier.[40] Almost all nitrogen isotherms show a gradual increase in the amount adsorbed up to the relative pressure of *ca.* 0.6–0.7 and later reach a plateau indicating a relatively small external surface. Only the adsorption isotherm for C_{AC}-1d, synthesized with acenaphthene, features an unusual shape that exhibits a very small micropore volume and a continuous increase in adsorption throughout the entire range of relative pressures. The hysteresis loops for the furfuryl alcohol-based carbons obtained from incompletely filled composites became more pronounced with increasing time of the hydrothermal treatment of the silica templates, which means an increase in the primary pore volume and correlates with results for the composites. Similarly as for the composites, the capillary evaporation occurs at the lower limit of adsorption–desorption

Table 4 Structural properties for the carbons studied from nitrogen adsorption data[a]

Sample	S_{BET}/ $m^2\ g^{-1}$	S_{ex}/ $m^2\ g^{-1}$	V_t/ $cm^3\ g^{-1}$	$V_p + V_{mi}$/ $cm^3\ g^{-1}$	w_{KJS}/ nm
C_{SU}-1d	1370	30	1.20	1.13	4.52
C_{FA2}-1d	1160	70	0.92	0.81	—
C_{AC}-1d	1260	[b]	1.68	[b]	~4.2
C_{FA1}-12h	1610	40	1.09	0.97	3.9[c]
C_{FA1}-1d	1670	80	1.32	1.19	4.7[c]
C_{FA1}-3d	1900	100	1.95	1.79	5.76
C_{FA1}-7d	2050	160	2.33	2.09	6.29

[a] S_{BET} = the BET specific surface area calculated in the range of relative pressures from 0.01 to 0.1, except the C_{AC}-1d carbon, for which calculation was done in the range from 0.1 to 0.25 due to the non-linearity of the BET plot; V_t = the total pore volume calculated at the relative pressure of about 0.98; $V_p + V_{mi}$ = the sum of the primary mesopore volume and micropore volume estimated by the α_s-plot method in the range of α_s from ~1.7 to 2.5; S_{ex} = the external surface area estimated by the α_s-plot method in the same range of α_s; w_{KJS} = the diameter of mesopores (formed by incomplete filling of the SBA-16 template) calculated using the KJS method.[63] [b] These quantities could not be evaluated by α_s-plot analysis due to the specific shape of the adsorption isotherm. [c] Approximate estimation from the shoulder on the PSD curve.

hysteresis with the exception of the C_{SU}-1d carbon, where this process starts already at the relative pressure of 0.56 and only part of the desorption branch can be attributed to the lower limit. This result seems to be consistent with the XRD pattern for the C_{SU}-1d and reveals not so dense formation of carbon walls for that type of precursor.

The pore size distributions for the carbons studied are shown in Fig. 8. The PSD curves for C_{FA2}-1d and C_{AC}-1d show one main peak, which is related to the mesopores created after dissolution of silica walls, whereas another irregular peak refers to microporosity. More interesting results were obtained for the furfuryl alcohol-based carbons obtained from the composites with incompletely filled mesopores of SBA-16. In this case two peaks or a peak and a shoulder are visible, which can be attributed to the pores created by dissolution of silica walls and the spherical pores arising from incomplete filling of the SBA-16 mesoporous cages. A comparison of the PSD curves shows more clearly a gradual shift of the peaks and an increase in the pore volume for the samples subjected to hydrothermal treatment. As can be noticed the second peak (and also shoulder, for which the position of the maximum is difficult to determine precisely, especially for C_{FA1}-12h), related to incompletely filled mesopores of SBA-16, is shifted to the lower values of the pore size in comparison to that for the composites. This finding may suggest that the hydrofluoric acid treatment of the silica template (acting as a support) could produce certain changes in the shape of pores causing some shrinkage of the carbon structure. In addition, this shrinkage was more pronounced for the samples obtained from the composites hydrothermally treated for shorter times, particularly C_{FA1}-12h and C_{FA1}-1d.

Table 2 and Table 5 contain information about thickness, t, determined by the XRD modeling for the composites and corresponding carbons. Noticeably, this thickness decreases from C_{FA1}/Al-SiO_2-7d (C_{FA1}-7d) to C_{FA1}/Al-SiO_2-12h (C_{FA1}-12h). It can be also speculated that the aforementioned decrease in the thickness of the carbon film

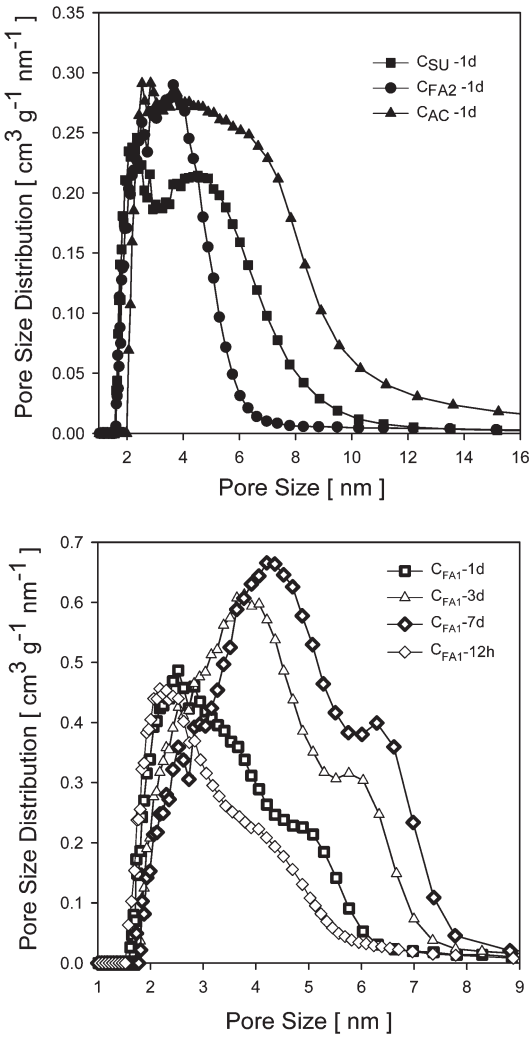

Fig. 8 Pore size distributions calculated from nitrogen adsorption isotherms for the carbons studied.

coated on the SBA-16 silica is related to the degree of shrinkage that occurs during the template removal. The latter effect is better visible in Fig. 9, which shows the normalized pore size distributions. The normalized PSD curves for the composites and corresponding carbons were calculated by dividing the PSD values by the BET specific surface area, which resulted in a dimensionless quantity. This normalization

Table 5 Structural characteristics of carbons synthesized using furfuryl alcohol carbon precursor determined by XRD modeling[a]

Sample	a/nm	D_i/nm	D_e/nm	w/nm	t/nm	ρ_1/ρ_2
C_{FA2}-1d	13.99	—	8.4	3.7	—	—
C_{FA1}-12h	11.97	7.2	8.4	2.0	0.63	2.0
C_{FA1}-1d	12.78	7.5	8.9	2.2	0.72	2.1
C_{FA1}-3d	15.05	7.9	9.7	3.3	0.91	2.0

[a] a = the cubic lattice parameter; D_i and D_e = the internal and external diameters of the spherical density areas (Fig. 1); w = the minimal distance between the surfaces of the spherical density areas given by $(a\sqrt{3}/2 - D_e)$; t = the thickness of the carbon nanosphere walls given by $(D_e - D_i)/2$; ρ_2/ρ_1 = the ratio between the averaged scattering densities of the carbon nanosphere walls and the interconnecting carbon material between the nanospheres (Fig. 1).

facilitates comparison of the volume of adsorbed nitrogen per squared meter of the accessible surface for both composites and carbons. As can be seen from this figure the effect of shrinkage is manifested by the pore size decrease for the carbons in comparison to the corresponding composite samples. The PSD analysis confirms the relatively high ratio of the single point total pore volume for C_{FA1} to that of C_{FA1}/Al-SiO_2, indicating a significant contribution of the porosity created after dissolution of the silica template. A possible interpretation of the normalized PSD curves for the C_{SU}-1d and C_{SU}/SiO_2-1d obtained by using sucrose as carbon precursor is that the HF acid treatment created some additional porosity by opening some intrinsic micropores in the carbon walls. Similarly as in the case of composite samples the size of spherical mesopores for the carbons studied estimated from the maximum of PSD is underestimated.

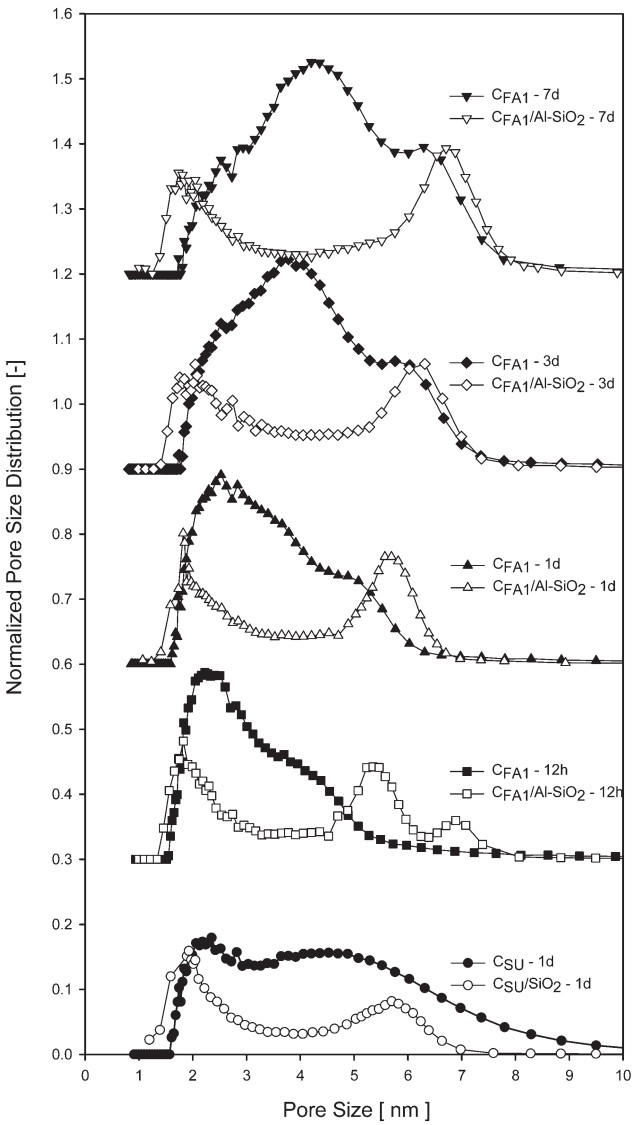

Fig. 9 Comparison of the normalized pore size distributions for the series of composite and carbon samples obtained from furfuryl alcohol; each pair of distributions, except the first one, is offset vertically by 0.3.

Fig. 10 shows the wide-angle XRD patterns for four carbon samples. The sharpness of the (002) peak decreases in the following order: C_{AC}-1d, C_{FA2}-1d, C_{FA1}-1d and C_{SU}-1d. The higher and sharper (002) and (101) peaks on the wide angle XRD pattern indicate a higher degree of graphitization of the carbon framework. In the case of C_{AC}-1d these peaks were much higher and narrower than those for other carbons obtained from sucrose and furfuryl alcohol, which form a rather amorphous carbon matrix. The (002) peak for C_{AC}-1d, $2\theta = 25.6^\circ$, corresponds to the carbon interlayer distance of 0.347 nm, which is slightly higher than that for graphite. The (002) peak for graphite is around $2\theta = 26.4^\circ$, which corresponds to the interlayer distance of 0.337 nm between the graphene sheets. Shown in Fig. 11, the TEM image and Fourier diffractogram along [111] incidence for C_{AC}-1d indicate high structural ordering of this carbon, which is the exact inverse replica of the SBA-16 silica template. Furthermore, the electron diffraction patterns indexed as [002], [101], and [110] show that the C_{AC}-1d carbon has more graphitic structure than the other carbons studied. However, the alignment of graphene sheets does not show some specific orientation such as that in CMK-3G, which was oriented perpendicularly to the direction of carbon rods.[46]

The SEM images for the carbon studied are shown in Fig. 12. The single crystal morphologies of carbon replicas are shown for C_{FA2}-1d, C_{AC}-1d, and C_{FA1}-1d. The C_{FA2}-1d, C_{FA1}-1d and C_{AC}-1d possess the same rhombdodecahedron single crystal

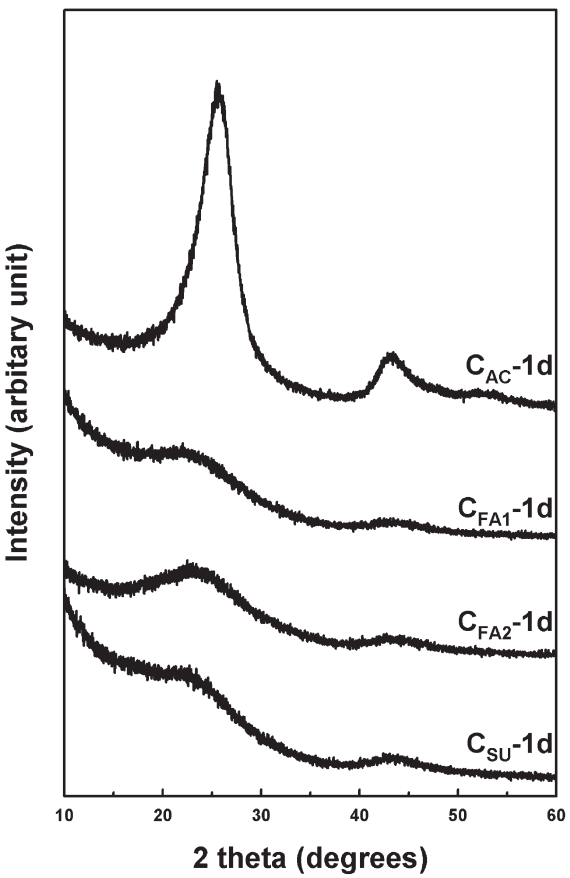

Fig. 10 Wide-angle XRD patterns for the carbon samples studied.

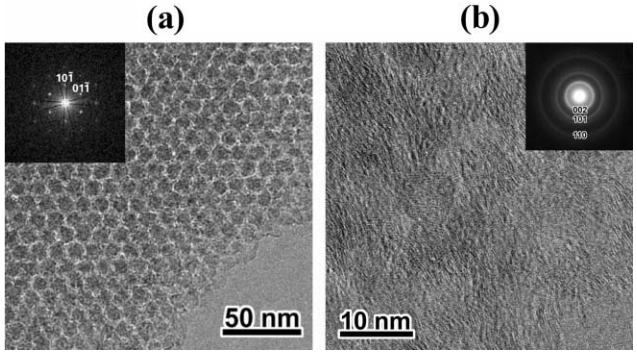

Fig. 11 TEM images of C_{AC}-1d carbon taken along [111] incidence. Low magnification image and corresponding Fourier diffractogram (FD) are shown in (a). Indices are based on mesostructure. Both image and FD clearly show the meso-scale order. High magnification TEM image and corresponding electron diffraction patterns are shown in (b). Indices are based on graphite.

shape morphology similar to the SBA-16 template. The preservation of crystal morphology during the SBA-16 templating synthesis of mesoporous carbons from furfuryl alcohol and acenaphthene provides additional confirmation that those carbons are faithful replicas of the SBA-16 template. However, the particles of C_{SU}-1d show completely shapeless morphologies due to the carbon deposition on these particles because sucrose does not fill uniformly the template mesopores and shows a tendency to deposit on the external surface of the silica template. In the case of C_{FA2}-1d some carbon deposition on the external surface of particles was observed and may be attributed to the addition of a second portion of furfuryl alcohol after initial pyrolysis at 623 K.

The TEM images are presented in Fig. 13 for C_{FA2}-1d and C_{FA1}-1d. These images show directly that C_{FA2}-1d is an exact inverse replica of the SBA-16 template with completely filled pores; however C_{FA1}-1d is an array of interconnected hollow carbon particles that are formed after coating the thin carbon film on the SBA-16 mesopore walls followed by silica dissolution.

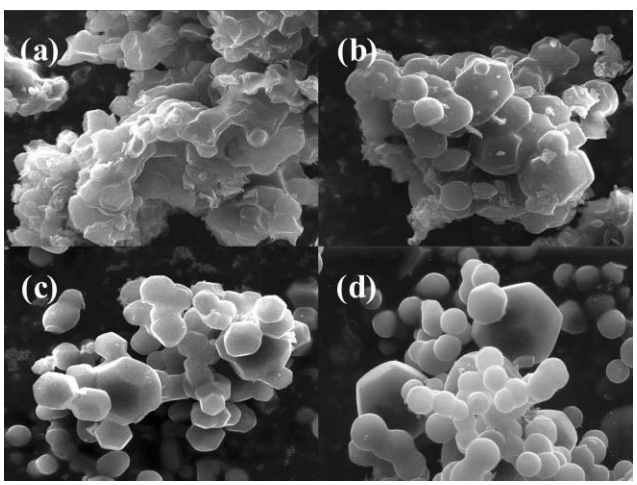

Fig. 12 SEM images for the carbon samples: (a) C_{SU}-1d, (b) C_{FA2}-1d, (c) C_{AC}-1d, and C_{FA1}-1d.

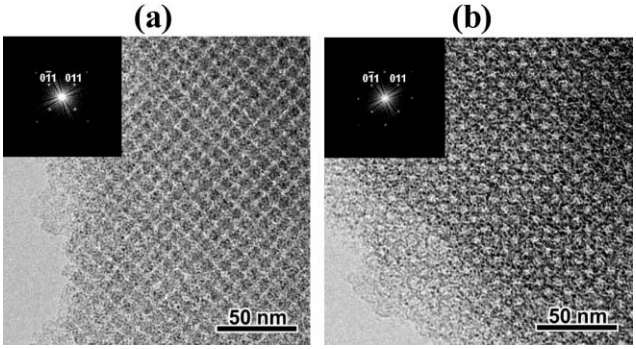

Fig. 13 TEM images for the (a) C_{FA2}-1d and (b) C_{FA1}-1d materials viewed along the [100] directions.

The density distribution in the carbons was simulated by spherical areas of variable density and diameters with the centers arranged in the vertices of the body centered cubic unit cell (see Fig. 1). These areas represent either the cavities of the SBA-16 template or carbon nanospheres for the carbon samples. Despite the simplicity of the density distribution model, its use in the synchrotron XRD structure modeling gave a good agreement between the experimental and calculated diffractograms as shown in Fig. 14 and 15. The structure parameters obtained by the synchrotron XRD modeling are summarized in Table 5.

The lattice parameters for the C_{FA1}-*t* samples are noticeably smaller than those for their respective SBA-16 templates. A comparison of the structure parameters for the C_{FA1}-*t* carbons and their Al-SiO_2-*t* templates in Table 5 shows that the lattice shrinkage of C_{FA1} takes place mainly in the region between the carbon nanospheres. The external diameters D_e for the carbon nanospheres of the C_{FA1} samples are virtually equal to the cavity diameters of their SBA-16 templates. However, the distances *w* between the carbon nanosphere surfaces for the C_{FA1} series are essentially smaller than the respective distances for the SBA-16 templates. Based on the above considerations we may assume that the shrinkage of the C_{FA1} carbons is due to their poor interconnectivity. It must be also noted that the relative structure shrinkage is smaller for the

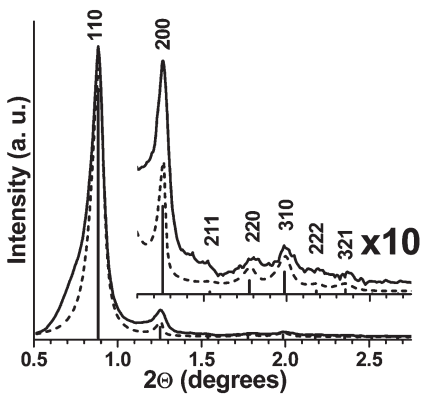

Fig. 14 Observed (solid line) and calculated (dotted line) synchrotron XRD profiles for the C_{FA2}-1d carbon sample. Calculated reflection positions are marked by dotted lines. The background curve is subtracted for clarity.

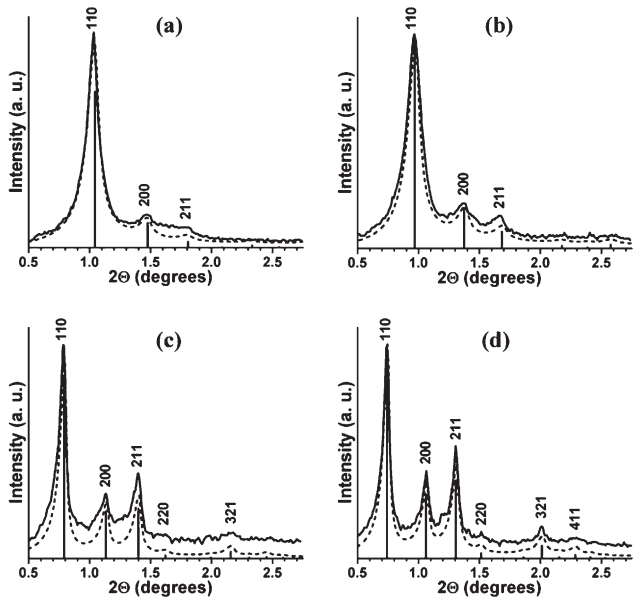

Fig. 15 Observed (solid line) and calculated (dotted line) synchrotron XRD profiles for hollow carbon samples: a) C_{FA1}-12h, b) C_{FA1}-1d, c) C_{FA1}-3d, and d) C_{FA1}-7d. Calculated reflection positions are marked by dotted lines. The background curve is subtracted for clarity.

C_{FA1} carbons synthesized from the SBA-16 templates subjected to longer hydrothermal treatment. In parallel, the XRD peaks for C_{FA1}-3d and C_{FA1}-7d carbons are distinctly sharper (Fig. 15), which is an indication of higher structural ordering for the carbons obtained by using templates after longer hydrothermal treatment. The discussed structure features may be explained by an increase in the interconnectivity between the SBA-16 cavities during the hydrothermal treatment process.

The C_{FA2}-1d sample demonstrates the same features, however its shrinkage is smaller, which may suggest its higher interconnectivity. The negligible lattice shrinkage of the C_{FA2}-1d carbon compared to C_{FA1}-1d can be related to the difference in their synthesis procedures. C_{FA2}-1d was synthesized applying double the amount of the carbon precursor, which could provide better filling of the SBA-16 mesopores and, consequently, better interconnectivity in the resulting mesostructured carbon.

4. Conclusions

Synthesis of mesoporous carbons with cubic $Im\bar{3}m$ structure was performed by employing SBA-16 mesoporous silica templates prepared by self-assembly of mixed triblock copolymers. Mesoporous carbons were prepared by carbonization of sucrose, furfuryl alcohol and acenaphthene used as carbon precursors. This study shows that sucrose is not suitable for the synthesis of cage-like carbons with cubic $Im\bar{3}m$ structure due to the intrinsic properties of sucrose-based carbon and the structural difficulty of fabricating a 3-D carbon network of spheres inside the SBA-16 template with relatively small interconnecting nanorods. Furfuryl alcohol was used to synthesize two types of mesoporous carbon with cubic $Im\bar{3}m$ structure. One of them was obtained by complete filling of the template mesopores, which led to the carbon with a single system of mesopores arising from the removal of silica walls. The other was prepared by coating a thin carbon film on the mesopore walls of the template, which resulted in the bimodal mesoporosity arising from silica walls and incompletely filled mesopores of SBA-16. The furfuryl alcohol-based mesoporous carbons exhibited very high BET specific surface area and high pore volumes. Moreover, in the case of bimodal distribution of mesopores their size could be controlled by varying the time of hydrothermal treatment of the SBA-16 template. The synthesis of mesoporous carbon from acenaphthene afforded materials with graphitic frameworks which show single mesoporosity and negligible microporosity, but the cubic $Im\bar{3}m$ structure was slightly deformed. This study shows that, by selection of the proper silica template and carbon precursor, the structural and adsorption properties of the resulting mesoporous carbons can be tailored to achieve different mesoporous structures with controlled microporosity and interconnectivity. Thus, this work shows how to tailor structural properties of carbons synthesized by using ordered silica as templates. In particular, the two kinds of separate mesoporous systems would provide new challenges and opportunities for supporting and/or incorporating host materials selectively to one of the pore systems and taking advantage of this approach in various applications such as adsorption and catalysis.

Acknowledgements

This work was supported in part by the donors of the Creative Research Initiative Program of the Korean Ministry of Science and Technology (R.R.), School of Molecular Science through the Brain Korea 21 project (R.R.), NSF Grant CHE-0093707 (M.J.), RFBR Grant 03-03-32127 (L.A.S.), the Swedish Research Council (O.T.), and Sweden and Japan Science and Technology Agency, Japan (O.T.).

Tae-Wan Kim,[a] Ryong Ryoo,*[a] Kamil P. Gierszal,[b] Mietek Jaroniec,[b] Leonid A. Solovyov,[c] Yasuhiro Sakamoto[d] and Osamu Terasaki[d]

[a]National Creative Research Initiative Center for Functional Nanomaterials and Department of Chemistry (School of Molecular Science BK21), Korea Advanced Institute of Science and Technology, Daejeon 305-701, Republic of Korea. E-mail: rryoo@kaist.ac.kr; Fax: (+82) 42 869 8130; Tel: (+82) 42 869 2830

[b]Department of Chemistry, Kent State University, Kent, OH 44242, USA

[c]Institute of Chemistry and Chemical Technology, 660049 Krasnoyarsk, Russia

[d]Structural Chemstry, Arrhenius Laboratory, Stockholm University, 10691 Stockholm, Sweden

References

1 S. A. Johnson, E. S. Brigham, P. J. Ollivier and T. E. Mallouk, *Chem. Mater.*, 1997, **9**, 2448.
2 T. Kyotani, T. Nagai, S. Inoue and A. Tomita, *Chem. Mater.*, 1997, **9**, 609.
3 R. Ryoo, S. H. Joo and S. Jun, *J. Phys. Chem. B*, 1999, **103**, 7743.
4 J. Lee, S. Yoon, T. Hyeon, S. M. Oh and K. B. Kim, *Chem. Commun.*, 1999, 2177.
5 J. H. Knox, B. Kaur and G. R. Millward, *J. Chromatogr.*, 1986, **352**, 3.
6 T. Kyotani, L.-F. Tsai and A. Tomita, *Chem. Mater.*, 1996, **8**, 2109.
7 R. Ryoo, S. H. Joo, M. Kruk and M. Jaroniec, *Adv. Mater.*, 2001, **13**, 677.

8 R. Ryoo and S. H. Joo, *Stud. Surf. Sci. Catal.*, 2004, **148**, 241.
9 T. Ohkubo, J. Miyawaki, K. Kaneko, R. Ryoo and N. A. Seaton, *J. Phys. Chem. B*, 2002, **106**, 6523.
10 S. Han, S. Kim, H. Lim, W. Choi, H. Park, J. Yoon and T. Hyeon, *Microporous Mesoporous Mater.*, 2003, **58**, 131.
11 W. S. Ahn, K. I. Min, Y. M. Chung, J.-K. Rhee, S. H. Joo and R. Ryoo, *Stud. Surf. Sci. Catal.*, 2001, **135**, 313.
12 J. Lee, S. Yoon, T. Hyeon, S. M. Oh and K. B. Kim, *Chem. Commun.*, 1999, 2177.
13 S. Yoon, J. Lee, T. Hyeon and S. M. Oh, *J. Electrochem. Soc.*, 2000, **147**, 2507.
14 S. H. Joo, S. J. Choi, I. Oh, J. Kwak, Z. Liu, O. Terasaki and R. Ryoo, *Nature*, 2001, **412**, 169.
15 J. Lee, S. Yoon, S. M. Oh, C.-H. Shin and T. Hyeon, *Adv. Mater.*, 2000, **12**, 359.
16 A.-H. Lu, W. Schmidt, A. Taguchi, B. Spliethoff, B. Tesche and F. Schuth, *Angew. Chem., Int. Ed.*, 2002, **41**, 3489.
17 M. Kang, S. H. Yi, H. I. Lee, J. E. Yie and J. M. Kim, *Chem. Commun.*, 2002, 1944.
18 J. S. Beck, J. C. Vartuli, W. J. Roth, M. E. Leonowicz, C. T. Kresge, K. D. Schmitt, C. T.-W. Chu, D. H. Olson, E. W. Sheppard, S. B. McCullen, J. B. Higgins and J. L. Schlenker, *J. Am. Chem. Soc.*, 1992, **114**, 10834.
19 A. Monnier, F. Schuth, Q. Huo, D. Kumar, D. Margolese, R. S. Maxwell, G. D. Stucky, M. Krishnamurty, P. Petroff, A. Firouzi, M. Janicke and B. F. Chmelka, *Science*, 1993, **261**, 1299.
20 L. A. Solovyov, V. I. Zaikovskii, A. N. Shmakov, O. V. Belousov and R. Ryoo, *J. Phys. Chem. B*, 2002, **106**, 12198.
21 M. Kaneda, T. Tsubakiyama, A. Carlsson, Y. Sakamoto, T. Ohsuna, O. Terasaki, S. H. Joo and R. Ryoo, *J. Phys. Chem. B*, 2002, **106**, 1256.
22 H. Yang, Q. Shi, X. Liu, S. Xie, D. Jiang, F. Zhang, C. Yu, B. Tu and D. Zhao, *Chem. Commun.*, 2002, 2842.
23 Q. Huo, D. I. Margolese, U. Ciesla, P. Feng, T. E. Gier, P. Sieger, R. Leon, P. M. Petroff, F. Schuth and G. D. Stucky, *Nature*, 1994, **368**, 317.
24 Y. Sakamoto, M. Kaneda, O. Terasaki, D. Y. Zhao, J. M. Kim, G. D. Stucky, H. J. Shin and R. Ryoo, *Nature*, 2000, **408**, 449.
25 R. Ryoo, S. H. Joo, S. Jun, T. Tsubakiyama and O. Terasaki, *Stud. Surf. Sci. Catal.*, 2001, **135**, 150.
26 D. Zhao, Q. Huo, J. Feng, B. F. Chmelka and G. D. Stucky, *J. Am. Chem. Soc.*, 1998, **120**, 6024.
27 R. Ryoo, C. H. Ko, M. Kruk, V. Antochshuk and M. Jaroniec, *J. Phys. Chem. B*, 2000, **104**, 11465.
28 M. Kruk, M. Jaroniec, C. H. Ko and R. Ryoo, *Chem. Mater.*, 2000, **12**, 1961.
29 M. Choi, W. Heo, F. Kleitz and R. Ryoo, *Chem. Commun.*, 2003, 1340.
30 S. Che, K. Lund, T. Tatsumi, S. Iijima, S. H. Joo, R. Ryoo and O. Terasaki, *Angew. Chem., Int. Ed.*, 2003, **42**, 2182.
31 S. Jun, S. H. Joo, R. Ryoo, M. Kruk, M. Jaroniec, Z. Liu, T. Ohsuna and O. Terasaki, *J. Am. Chem. Soc.*, 2000, **122**, 10712.
32 H. J. Shin, R. Ryoo, M. Kruk and M. Jaroniec, *Chem. Commun.*, 2001, 349.
33 S. H. Joo, R. Ryoo, M. Kruk and M. Jaroniec, *J. Phys. Chem. B*, 2002, **106**, 4640.
34 J.-S. Lee, S. H. Joo and R. Ryoo, *J. Am. Chem. Soc.*, 2002, **124**, 1156.
35 L. A. Solovyov, A. N. Shmakov, V. I. Zaikovskii, S. H. Joo and R. Ryoo, *Carbon*, 2002, **40**, 2477.
36 M. Kruk, M. Jaroniec, S. H. Joo and R. Ryoo, *J. Phys. Chem. B*, 2003, **107**, 2205.
37 S.-S. Kim and T. J. Pinnavaia, *Chem. Commun.*, 2001, 2418.
38 C. Yu, J. Fan, B. Tian, D. Zhao and G. D. Stucky, *Adv. Mater.*, 2002, **14**, 1742.
39 W.-H. Zhang, C. Liang, H. Sun, Z. Shen, Y. Guan, P. Ying and C. Li, *Adv. Mater.*, 2002, **14**, 1776.
40 M. Kruk, M. Jaroniec, T.-W. Kim and R. Ryoo, *Chem. Mater.*, 2003, **15**, 2815.
41 H. Darmstadt, C. Roy, S. Kaliaguine, T.-W. Kim and R. Ryoo, *Chem. Mater.*, 2003, **15**, 3300.
42 L. A. Solovyov, T.-W. Kim, F. Kleitz, O. Terasaki and R. Ryoo, *Chem. Mater.*, 2004, **16**, 2274.
43 F. Kleitz, S. H. Choi and R. Ryoo, *Chem. Commun.*, 2003, 2136.
44 S. Che, A. E. Garcia-Bennett, X. Liu, R. P. Hodgkins, P. A. Wright, D. Zhao, O. Terasaki and T. Tatusmi, *Angew. Chem., Int. Ed.*, 2003, **42**, 3930.
45 Y. Sakamoto, T.-W. Kim, R. Ryoo and O. Terasaki, *Angew. Chem., Int. Ed.*, 2004, **43**, 5231.
46 T.-W. Kim, I.-S. Park and R. Ryoo, *Angew. Chem., Int. Ed.*, 2003, **42**, 4375.
47 C. Vix-Guterl, S. Saadalladh, L. Vidal, M. Reda, J. Parmentier and J. Patarin, *J. Mater. Chem.*, 2003, **13**, 2535.
48 Z. Li and M. Jaroniec, *J. Phys. Chem. B*, 2004, **108**, 824.
49 P. Van Der Voort, M. Benjelloun and E. F. Vansant, *J. Phys. Chem. B*, 2002, **106**, 9027.
50 F. Kleitz, D. Liu, G. M. Anilkumar, I.-S. Park, L. A. Solovyov, A. N. Shmakov and R. Ryoo, *J. Phys. Chem. B*, 2003, **107**, 14296.
51 F. Kleitz, L. A. Solovyov, G. M. Anilkumar, S. H. Choi and R. Ryoo, *Chem. Commum.*, 2004, 1536.
52 T. Yamada, H. S. Zhou, H. Uchida, M. Tomita, Y. Ueno, T. Ichino, I. Honma, K. Asai and T. Katsube, *Adv. Mater.*, 2002, **14**, 812.
53 R. Ryoo, S. Jun, J. M. Kim and M. J. Kim, *Chem. Commun.*, 1997, 2225.
54 M. S. Morey, A. Davidson and G. D. Stucky, *J. Porous Mater.*, 1998, **5**, 195.
55 H. M. Hunter and P. A. Wright, *Microporous Mesoporous Mater.*, 2001, **43**, 361.
56 L.-X. Dai, Y.-H. Teng, K. Tabata, E. Suzuki and T. Tatsumi, *Microporous Mesoporous Mater.*, 2001, **44–45**, 573.
57 L.-X. Dai, K. Tabata, E. Suzuki and T. Tatsumi, *Chem. Mater.*, 2001, **13**, 208.
58 Y.-J. Han, J. T. Watson, G. D. Stucky and A. Butler, *J. Mol. Catal. B: Enzym.*, 2002, **17**, 1.
59 B. Tian, X. Liu, B. Tu, C. Yu, J. Fan, L. Wang, S. Xie, G. D. Stucky and D. Zhao, *Nature Mater.*, 2003, **2**, 159.
60 J. Fan, C. Yu, L. Wang, Y. Sakamoto, O. Terasaki, B. Tu and D. Zhao, *Stud. Surf. Sci. Catal.*, 2003, **416**, 97.
61 T.-W. Kim, R. Ryoo, M. Kruk, K. Gierszal, M. Jaroniec, S. Kamiya and O. Terasaki, *J. Phys. Chem. B*, 2004, **108**, 11489.
62 S. Jun and R. Ryoo, *J. Catal.*, 2000, **195**, 237.
63 K. S. W. Sing, D. H. Everett, R. A. W. Haul, L. Moscou, R. A. Pierotti, J. Rouquerol and T. Siemieniewska, *Pure Appl. Chem.*, 1985, **57**, 603.
64 M. Kruk, M. Jaroniec and K. P. Gadkaree, *J. Colloid Interface Sci.*, 1997, **192**, 250.
65 M. Kruk and M. Jaroniec, *J. Phys. Chem. B*, 2002, **106**, 4732.
66 M. Kruk, M. Jaroniec and A. Sayari, *Langmuir*, 1997, **13**, 6267.
67 L. A. Solovyov, S. D. Kirik, A. N. Shmakov and V. N. Romannikov, *Microporous Mesoporous Mater.*, 2001, **44–45**, 17; L. A. Solovyov, S. D. Kirik, A. N. Shmakov and V. N. Romannikov, *Adv. X-ray Anal.*, 2001, **44**, 110.
68 L. A. Solovyov, *J. Appl. Crystallogr.*, 2004, **37**, 743.
69 H. M. Rietveld, *J. Appl. Crystallogr.*, 1969, **2**, 65.
70 D. B. Wiles and R. A. Young, *J. Appl. Crystallogr.*, 1981, **14**, 149.
71 C. Yu, J. Fan, B. Tian, G. D. Stucky and D. Zhao, *J. Phys. Chem. B*, 2003, **107**, 13368.
72 C. Yu, B. Tian, J. Fan, G. D. Stucky and D. Zhao, *J. Am. Chem. Soc.*, 2002, **124**, 4556.